J Mater Sci: Mater Med (2008) 19:1097–1108
DOI 10.1007/s10856-007-3044-3

In vivo behavior of bioactive phosphate glass-ceramics from the system P_2O_5–Na_2O–CaO containing TiO_2

Ahmed Soltan Monem · Hatem A. ElBatal · Elsayed M. A. Khalil · Moenis A. Azooz · Yousry M. Hamdy

Received: 20 February 2006 / Accepted: 5 May 2006 / Published online: 15 August 2007

Abstract Soda lime phosphate bioglass-ceramics with incorporation of small additions of TiO_2 were prepared in the metaphosphate and pyrophosphate region, using an appropriate two-step heat treatment of controlled crystallization defined by differential thermal analysis results. Identification and quantification of crystalline phases precipitated from the soda lime phosphate glasses were performed using X-ray diffraction analysis. Calcium pyrophosphate (β-$Ca_2P_2O_7$), sodium metaphosphate ($NaPO_3$), calcium metaphosphate (β-$Ca(PO_3)_2$), sodium pyrophosphate ($Na_4P_2O_7$), sodium calcium phosphate ($Na_4Ca(PO_3)_6$) and sodium titanium phosphate ($Na_5Ti(PO_4)_3$) phases were detected in the prepared glass-ceramics. The degradation of the prepared glass-ceramics were carried out for different periods of time in simulated body fluid at 37 °C using granules in the range of (0.300–0.600 mm). The released ions were estimated by atomic absorption spectroscopy and the surface textures were measured by scanning electron microscopy. Evaluation of in vivo bioactivity of the prepared glass-ceramics was carried through implanting the samples in the rabbit femurs. The results showed that the addition of 0.5 TiO_2 mol% enhanced the bioactivity while further increase of the TiO_2 content decreased the bioactivity. The effect of titanium dioxide on the bioactivity was interpreted on the basis of its action on the crystallization process of the glass-ceramics.

A. S. Monem
Biophysics Department, Faculty of Science, Cairo University, Cairo, Egypt

H. A. ElBatal · M. A. Azooz
Glass Research Department, National Research Center, Dokki, Cairo, Egypt

E. M. A. Khalil · Y. M. Hamdy (✉)
Spectroscopy Department, National Research Center, Dokki, Cairo, Egypt
e-mail: yousry_m_h@yahoo.com

Introduction

Phosphate based glasses have found considerable use in various applications such as glass to metal seals, low-temperature enamels for metals, optical elements, hosts for radioactive wastes management, and as biomaterials [1–3]. The quite high solubility can be changed or controlled by the doping of the glass with various ions such as Al^{3+}, Pb^{2+}, or B_2O_3 [4]. The increase of chemical durability is achieved by the increase of the cross-linkage or the introduction of highly insoluble ions and this makes the glass structure less susceptible to solution attack [5].

Recent studies on phosphate based glasses have shown that the useful range of such glasses [6] to biomedical applications is limited not only by crystallization effects, but also in vitro studies have shown that too high solubility is detrimental to cell activity [7]. Franks et al. [6] have shown that glasses with a fixed P_2O_5 content of 45 mol% give a good range of glasses which melt and cast easily and show good biocompatibility as a biomaterial in vitro.

Titanium dioxide is considered to be harmless in contact with human tissue and it has thus gained interest in the production of bioactive SiO_2–CaO–P_2O_5 glass-ceramics [8–10]. TiO_2, used as a nucleating agent, in glasses, is miscible in the glassy network at high temperatures but induces phase separation during cooling of the melt [8, 9]. The role of TiO_2 in bioactive glasses and glass-ceramics is still in debate. Titanium dioxide is known to induce calcium-phosphate volume crystallization in CaO–P_2O-based systems [11].

Hosono et al. [12, 13] used significant amounts of TiO_2 to produce porous glass-ceramics in which the volume nucleated β-$Ca_3(PO_4)_6$ phase was leached with HCl leaving a $CaTi_4(PO_4)_6$ skeleton. Ceramming of glasses in this system usually gives rise to biocompatible phases, such as β-$Ca_2P_2O_7$ and $Ti_2P_2O_7$. Lacerda et al. [14] found that TiO_2 contents up to 3 wt% produce crystallization of SiO_2–$3CaO{\cdot}P_2O_5$–MgO glasses.

Kasuga et al. [15, 16] examined the glass-ceramic derived from $60CaO–30P_2O_5–7Na_2O–3TiO_2$ glass and found that it showed bioactivity. Grussaute et al. [17] studied by MAS NMR glasses of the system $Na_2O–TiO_2–P_2O_5–SiO_2$ and the results reveal the formation of Ti–O–P covalent bonds, owing to the electrostatic field strength of Ti^{4+} ions. Navarro et al. [18] studied the degradation of TiO_2-stabilized of phosphate glasses and showed that the addition of TiO_2 in this glass system enhanced the chemical durability towards deionized water and simulated body fluid due to the presence of Ti–O–P bonds rather than P–O–P bonds and Raman spectra indicate the presence of TiO_5 and TiO_6 groups.

Calcium phosphate-based glasses and bioceramics are designed to degrade gradually over time and be replaced by the natural host tissue. The prime objective for such materials in vivo is to combine stimulation of osteogenic activity in associated bone tissues for optimum healing, with the capability to be progressively resorbed by specialized bone cells (osteoclasts) during normal continuous remodeling [19]. Kotani et al. [20] and Neo et al. [21] studied the difference in bone-bonding mechanisms between surface-active ceramics and bioresorbable ceramics. They found that the surface-active ceramic was bonded to bone through a thin Ca–P rich layer consisting of fine apatite crystals apparently different from those of bone in shape, size, and orientation. The resorbable ceramics made direct contact with the bone, and no apatite layer was present at the interface. The surfaces of the implants became rough due to degradation, and bone grew into the finest surface irregularities.

The first objective of this work is to study the in vivo behavior of some bioglass-ceramics from the system P_2O_5–Na_2O–CaO to which few successive percents of TiO_2 were added. The second objective is to characterize the glass-ceramic samples by scanning electron microscopy and X-ray diffraction analysis to analyze the role of TiO_2 in such bioglass-ceramics.

Materials and methods

Glass preparation

Six glasses were prepared from chemically pure $CaCO_3$, Na_2CO_3, $NH_4H_2PO_4$, and TiO_2 (see Table 1 for their compositions). The batches were weighed out and then melted in porcelain crucibles in an electric furnace between 1,100 and 1,200 °C for 2 h and the melts were rotated two times to achieve homogeneity. Upon complete melting, the glasses were cast in a preheated stainless steel rectangular mould of the dimensions of $1 \times 4 \times 1$ cm^3 preheated to about 250 °C. The glass samples were transferred to an annealing muffle furnace adjusted at 350 °C and the muffle was left to cool slowly to room temperature at a rate of 25 °C/h.

Table 1 Phosphate bioglass samples compositions

Name	mol%			
	P_2O_5	CaO	Na_2O	TiO_2
P1	45	24	31.0	–
P2	45	24	30.5	0.5
P3	45	24	30.0	1.0
P4	45	24	29.5	1.5
P5	45	24	29.0	2.0
P6	45	24	28.5	2.5

Differential thermal analysis

Differential thermal analysis (DTA) measurements were carried out on powdered samples which were examined up to 700 °C using a recording DTA apparatus Setaram (France) and alumina was used as a reference material.

Preparation of glass-ceramic samples (Heat treatment regime)

Based on the thermal data obtained from differential thermal analysis measurements, the specific temperatures necessary for controlled thermal heat treatment regime are obtained. The heat-treatment schedule consists of two-steps regime, the first temperature is equivalent for efficient nucleation step and the second temperature is equivalent to the maximum crystal growth step and the two selected temperatures are generally correlated with endothermic and exothermic peaks of the DTA thermogram. For all samples, the time of holding at the first nucleation temperature was taken as 24 h to ensure maximum nuclei, while the time of the crystallization step was taken as 12 h. The two-steps heat-treatment regime was done in a regulated muffle furnace (Carbolite, England). The glass specimens were heated slowly to the first nucleation temperature at a rate of 3 °C/min. After holding for 24 h at the specified temperature, the muffle temperature was raised to reach the second crystallization temperature at a rate of 3 °C/min and after a second hold for 12 h, the muffle was switched off and the samples were left to cool inside the muffle to room temperature at a rate of 20 °C/h. The prepared glass-ceramic samples were polished by 600-grit paper, 1200-grit and

2500-grit silicon carbide powders and a final polish was done by cerium oxide.

Characterization of bioglass-ceramics

X-ray diffraction measurements

The prepared glass-ceramic samples were finely ground and the fine powder was examined using a Brukur D8 Advance X-ray diffractometer (Germany) adopting Ni-filter and Cu-target to identify the precipitated crystalline phases.

Microstructure measurements using scanning electron microscope

The surface textures of the prepared glass-ceramic samples were examined using a scanning electron microscope type JEOL, JXA-840A (Japan) after coating with gold using Edwards S 150A sputter coater (England).

Corrosion studies using atomic spectroscopy

The glass-ceramic samples, in the form of grains in the size range (0.300–0.600 mm), were subjected to the action of the simulated body fluid (SBF), prepared according to Kokubo et al. [22], at temperature of 37 °C for different periods of time. About 0.25 g of each sample grains was weighed accurately and was put in a polyethylene container. 25 mL of SBF was poured on the grains and the container was covered and put in an incubator adjusted to 37 °C. The containers were removed from the incubator at time periods 3 h, 6 h, 1 day, 3 days, 1 week and 2 weeks. Each sample was tested 3 times for each time period. The solution of SBF was filtered on ashless filter paper no. 41.

Measurement of calcium, and sodium ions by atomic absorption spectroscopy (AAS): The attacking solutions were diluted with deionized water as follows: 10 times for calcium ions concentration measurement, 100 times for sodium ions concentration measurements. The SBF solution was also diluted with the deionized water and was measured with the samples. The concentration measurements for calcium, sodium ions were done on Varian Spectra AA 220 atomic absorption spectrometer with deuterium (D_2) lamp, background correction was used. Also, hollow cathode lamps were used and all the measurements were performed in the background-corrected peak-area measurement mode. The elements were determined using the flame atomic absorption spectroscopy in acetylene–air or acetylene–nitrous oxide flames. The calibration was performed using multi-element calibration solutions prepared from 1,000 mg/L stock solutions (Merck). Sodium ions are measured using acetylene- air flame at wavelength 330.3 nm, slit width 0.2 nm, and lamp current 7 mA. Calcium ions are measured using acetylene-nitrous oxide flame at wavelength 239.9 nm, slit width 0.2 nm, and lamp current 6 mA.

Measurement of phosphorous ions by induced coupled plasma atomic emission spectroscopy (ICP-AES): The solutions of the samples were diluted 10 times by deionized water. The SBF solution was measured with the samples. The phosphorous 214 nm spectral line was utilized for the measurements. The calibration was performed using calibration solution prepared from 1,000 mg/L stock solution (Merck).

Evaluation of in vivo bioactivity of glass-ceramics

Surgical procedure

Adult male New Zealand white rabbits weighing about 3 kg were used as the animal model. Three animals were used for each glass-ceramic sample. Animals were anesthetized with a cocktail of 5 mL of ketamine (100 mg/cc) + 2.5 mL of xylazine (20 mg/cc), administered intramuscularly (IM) at dose of 1 mL/kg body weight. The animals were also given an intramuscular prophylactic dose of penicillin G (25,000 U/kg) to reduce the risk of infection. The surgical site was shaved and prepared with a solution of betadine (Povidone–iodine) and alcohol. Under the sterile surgical conditions, the skin over the anteromedical aspect of each femoral diaphysis was incised and the skin and periosteum was retracted so that the femur bone can be exposed. A mid-shaft femoral cortical bone defect (6 mm in diameter) was created in the anteromedical aspect of each femur using a low-speed dental burr under continuous rinsing by cold physiologic saline solution to minimize heat related damage, and to remove all the bone particles. The bone marrow chamber was evacuated by repeated washings with saline solution through a syringe introduced into the defect space. The surgical site was packed with gauze until bleeding subsided. Immediately following, the granules of prepared glass-ceramic (0.300–0.600 mm) were placed in sufficient amounts to fill the holes, then the periosteum muscle and skin were sutured in layer, some holes were left empty as control. After 6 weeks post surgery, the animals were sacrificed and the bone segments containing the defects were bisected and fixed in 4% phosphate-buffered formaldehyde solution (pH 7.2) for 24 h.

Histological method

The specimens were decalcified in 10% ethylene diamine tetra acetic acid solution (EDTA), pH 7.4 for 14 days. The specimens were dehydrated in serial alcohol solutions and mounted in paraffin, cut cross sectional into slices of 4 μm thickness and stained with hematoxylin-eosin. The samples were examined under light microscope at different magnifications.

Results

Characterization of bioglass-ceramic samples

Differential thermal analysis

Differential thermal analysis results are shown in Fig. 1 for phosphate bioglasses. The results reveal that the nucleation and crystallization temperatures increase with the increase of TiO_2 content for the phosphate bioglasses. The nucleation and crystallization temperatures for the samples are shown in Table 2.

X-ray diffraction results for bioglass-ceramics

Figure 2 shows the X-ray diffraction patterns for the phosphate bioglass-ceramic samples. The X-ray diffraction patterns of the reference sample P1, which contains no TiO_2, shows the presence of the following crystalline phases:

a) Calcium pyrophosphate β-$Ca_2P_2O_7$ (card number: 9-346)
b) Sodium metaphosphate $NaPO_3$ (card number: 2-776)
c) Calcium metaphosphate β-$Ca(PO_3)_2$ (card number: 17-500)
d) Sodium pyrophosphate $Na_4P_2O_7$ (card number: 10-187)
e) Sodium calcium phosphate $Na_4Ca(PO_3)_6$ (card number: 25-0811)

Careful inspection of the diffraction patterns indicates that the peak intensities of the crystalline phases show that calcium pyrophosphate is the main crystalline phase, then both sodium metaphosphate and calcium metaphosphate are found in considerable amounts while sodium pyrophosphate and sodium calcium phosphate are found in small amounts.

The evolution of the X-ray peaks with the increase of TiO_2 content from sample P2 to sample P6 reveals that the crystalline phases of sodium metaphosphate and calcium metaphosphate decrease with the increase of TiO_2 content except in sample P5 where the peak intensities of the sodium metaphosphate phase are still high as in sample P1. The peak intensities of the crystalline phase of sodium calcium phosphate are disappeared in all the samples containing TiO_2 (P2–P6). The peak intensities of crystalline sodium pyrophosphate phase become very weak in the samples (P2–P6). With the increase of the TiO_2 content, a new phase is formed beginning from sample P2 with small peak intensities and continues to grow. The new phase is attributed to sodium titanium phosphate $Na_5Ti(PO_4)_3$ (card number: 39-178). The peak intensities of the new-formed phase reach their maximum values in the sample P5, and then they slightly decrease in the sample P6.

Scanning electron microscope investigations

Figure 2 shows the micrographs of the phosphate bioglass-ceramic samples. The morphological structure varies with

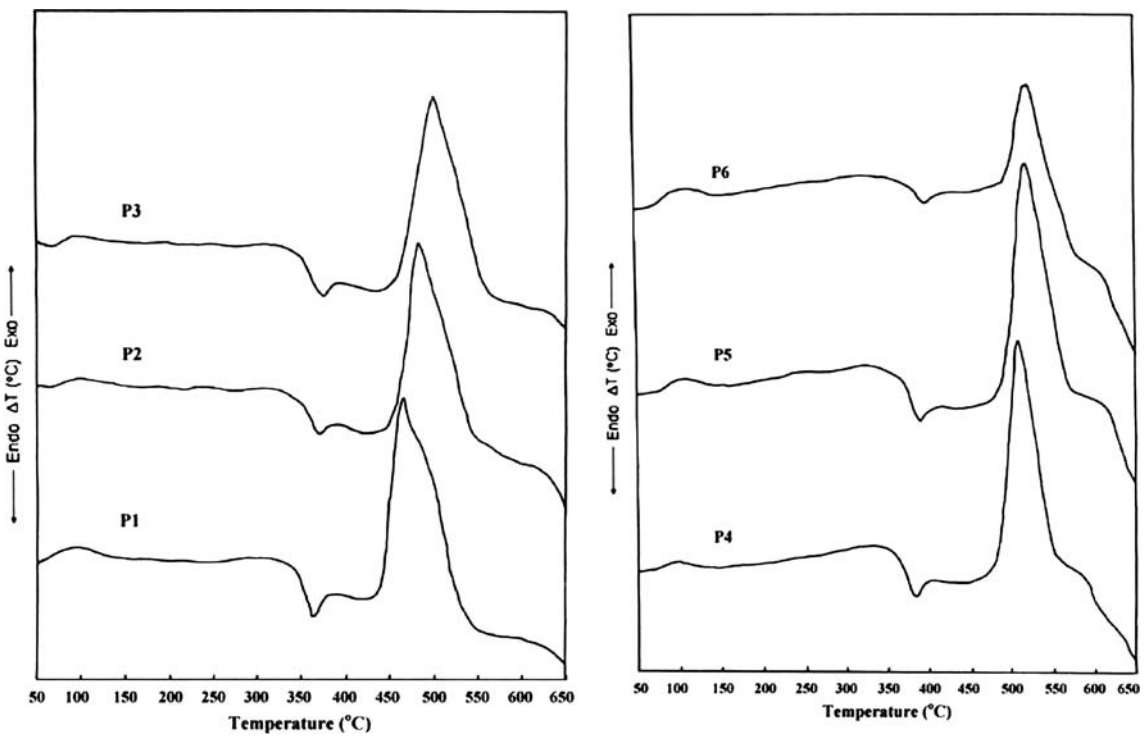

Fig. 1 Differential thermal analysis curves for the phosphate bioglass samples at a heating rate of 10 °C/min

Table 2 Nucleation and crystallization Peaks for the phosphate bioglasses

Sample	Nucleation Temperature (°C)	Crystallization Temperature (°C)
P1	364	461
P2	371	479
P3	375	500
P4	380	502
P5	384	509
P6	386	511

the composition of the samples. All the samples show almost complete crystallization. The base glass-ceramic sample P1 shows rounded crystals of the diameter 10 μm. Increasing the TiO_2 content causes gradual decrease in the dimension of the crystals.

Corrosion results (elemental concentration analysis)

The elemental concentration analysis data obtained after the immersion in the simulated body fluid of phosphate bioglass-ceramics for prolonged times can be outlined as follows:

Figure 3 reveals the phosphorous ion concentration estimated after the immersion of the phosphate glass-ceramic samples for different reaction times. It is obvious that after 3 h of immersion, the phosphorous ion concentration sharply increases for all studied samples and with prolonged times the quantity estimated is shown to approach the double after 72 h and approaches almost saturation afterwards.

Figure 4 reveals the sodium ions concentration estimated for phosphate bioglass-ceramic samples after the immersion for prolonged times in SBF at 37 °C. The amount of released sodium ions progressively increases with time of immersion and the differences between the various bioglass-ceramic samples are small.

Figure 5 reveals the estimated calcium ions concentration released from phosphate bioglass-ceramic samples after the immersion in SBF for prolonged times at 37 °C. The bioglass-ceramics show peculiar behavior by showing a high increase of the amounts released until reaching 6 h of immersion. Further immersion, reveals a slower rate of decrease in the amounts of calcium ions.

Histological results of in vivo bioactivity of bioglass-ceramic samples.

Figure 6 shows a histological section of a critical size bone defect created in a rabbit femur and grafted with P1

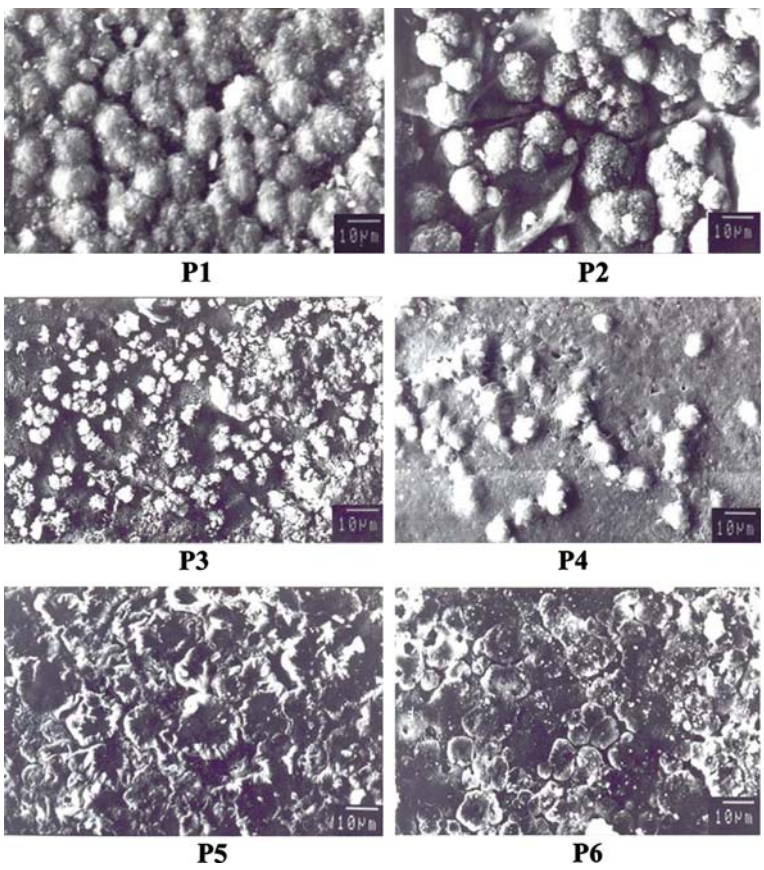

Fig. 2 Scanning electron micrographs for the bioglass-ceramic samples at magnification 1,000×

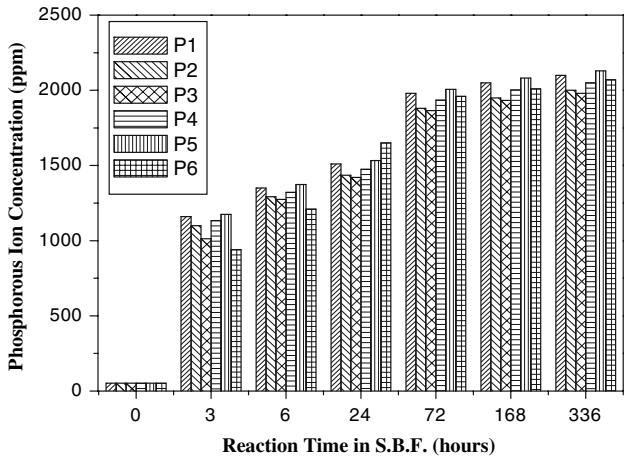

Fig. 3 Phosphorous ion concentration released from the bioglass-ceramic samples in reacted SBF after different time periods at 37 °C

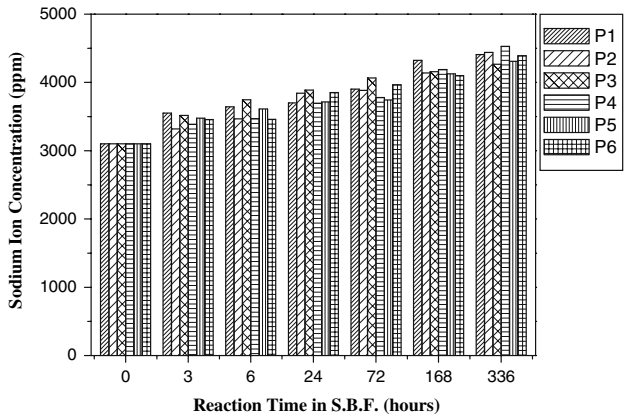

Fig. 4 Sodium ion concentration released from the bioglass-ceramic samples in reacted SBF after different time periods at 37 °C

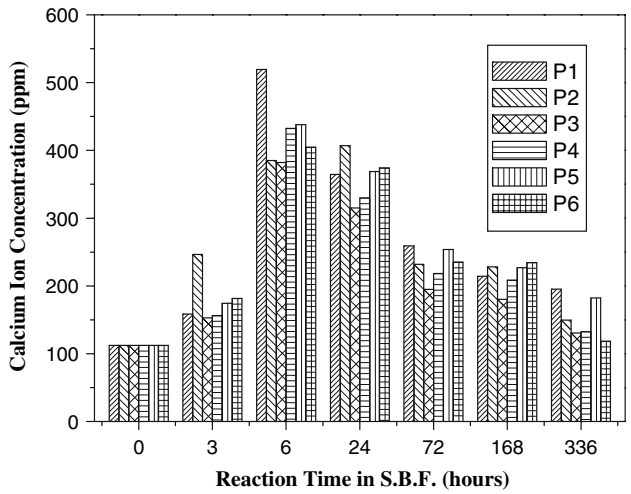

Fig. 5 Calcium ion concentration released from the bioglass-ceramic samples in reacted SBF after different time periods at 37 °C

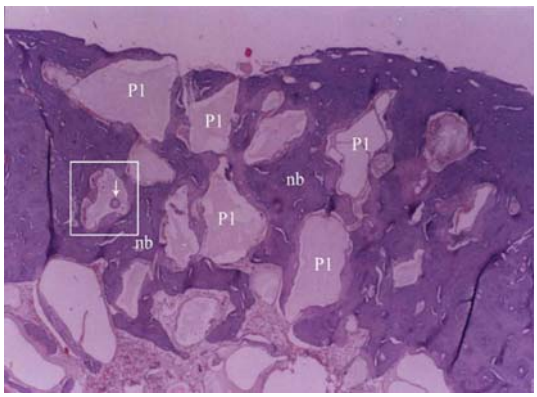

Fig. 6 Histological section of a critical size bone defect created in the rabbit femur and grafted with P1 particles 6 weeks post surgery, new bone tissue (nb) was seen filling the inter-space between the P1 particles. The in-growing bone was observed in close contact with the particles, without an intervening fibrous tissue layer. Furthermore, no sign of inflammatory cell infiltration at the implantation site were seen. Moreover, bone formation was also found on the surface of P1 particles as indicated by arrows (Hematoxylin—eosin stain), original magnification 40×

particles. New bone tissue with osteocyte embeded in lacuna is seen filling the inter-space between the P1 particles. The in-growing bone is observed in close contact with the particles, without an intervening fibrous tissue layer. Furthermore, the newly formed bone is barely distinguishable from the host bone and no sign of inflammatory cell infiltration at the implantation site are seen. Moreover, bone formation is also found on the surface of P1 particles,

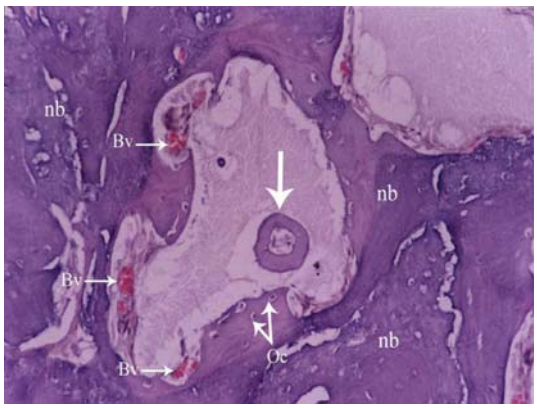

Fig. 7 A magnified image for the area inside the box in Fig. 6, showing one P1 particle which is surrounded completely by new bone (nb) with osteocyte (Oc) embeded in lacuna. In addition, several blood vessels (Bv) filled with red blood cells were seen throughout the regenerated bone and in close contact with P1 particle. This indicate that the regenerated bone is highly vascularized. Furthermore, bone formation was also seen on the surface of P1 particle as indicated by arrow. (Hematoxylin—eosin stain), original magnification 200×

as shown in Fig. 7. In addition, several blood vessels filled with red blood cells are seen throughout the regenerated bone and in close contact with P1 particle . This indicates that the regenerated bone is highly vascularized and it is very well supplied with blood, which contains oxygen, fresh tissue fluid, nutrients and growth factors needed for the bone regeneration, as shown in Fig. 7.

Figure 8 shows histological section of a critical size bone defect created in a rabbit femur and grafted with P2 particles. New bone tissue with osteocyte embeded in lacuna is seen filling the inter-space between the P2 particles. The in-growing bone is observed in close contact with the particles, without an intervening fibrous tissue layer. Furthermore, the entrances to the osseous defect are almost entirely closed after 6 weeks and the newly formed bone is barely distinguishable from the host bone, no sign of inflammatory cell infiltration at the implantation site are seen. Moreover, bone formation is also found on the surface of P2 particles as shown in Figs. 9–11. In addition, a developing osteon is also seen on the surface of P2 particle which possesses a central haversian canal passing through P2 particle and lining with osteoblast, this canal is also containing blood vessels (Fig. 10). This result suggests that osteoclast is mediating material resorption to form a new resorption tunnel or canal which passes through the grafted material, this process is followed by bone apposition by osteoblasts that start building up a new osteon within the tunnel. As a result of these two processes P2 will gradually be resorbed and became replaced by new bone, this is very similar to normal bone remodeling.

Figure 12 shows a histological section of a critical size bone defect created in a rabbit femur and grafted with P3 particles. New bone tissue with osteocyte embeded in lacuna is seen filling the inter-space between the P3 particles. The in-growing bone is observed in close contact with the particles, without an intervening fibrous tissue layer. Furthermore, the newly formed bone is barely distinguishable from the host bone and no sign of inflammatory cell infiltration at the implantation site are seen. In addition, the entrances to the osseous defect are almost entirely closed after six weeks as seen in Fig. 12. Moreover, no bone formation is observed on the surface of P3 particles as in the case of P1 and P2 (Fig. 13). The same features were found to be repeated with the samples P4, P5, and P6.

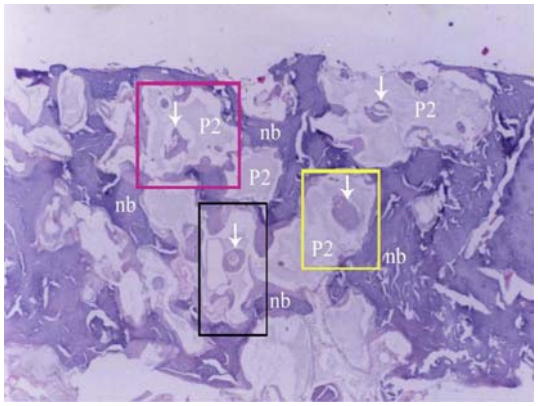

Fig. 8 Histological section of a critical size bone defect created in the rabbit femur and grafted with P2 particles 6 weeks post surgery, new bone tissue (nb) was seen filling the inter-space between the P2 particles. The in-growing bone was observed in close contact with the particles, without an intervening fibrous tissue layer. Furthermore, no sign of inflammatory cell infiltration at the implantation site were seen. Moreover, bone formation was also found on the surface of P2 particles as indicated by arrows. (Hematoxin—eosin stain), original magnification 40×

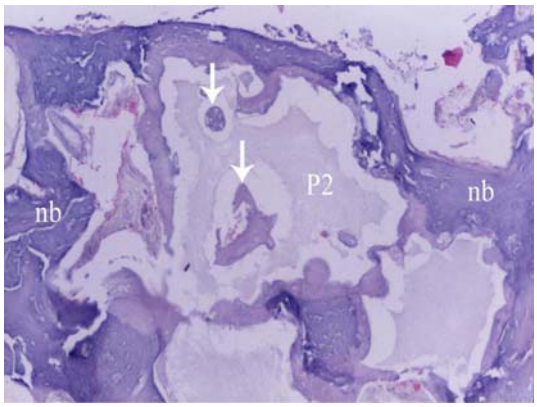

Fig. 9 A magnified image for the area inside the red box in Fig. 8, showing bone formation on the surface of P2 particle as indicated by arrows (Hematoxylin—eosin stain), original magnification 100×

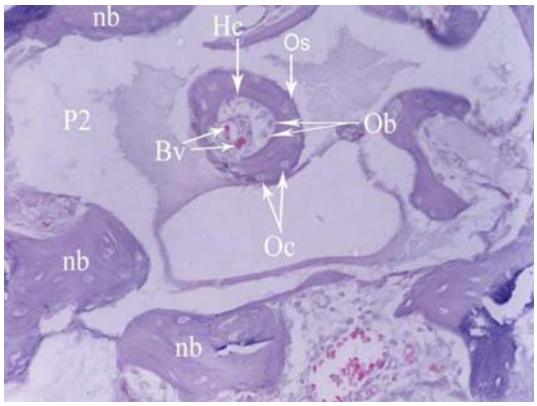

Fig. 10 A magnified image for the area inside the black box in Fig. 8, showing one P2 particle which is surrounded by new bone (nb) with osteocyte (Oc) embeded in lacuna. Furthermore, a developing osteon (Os) was also seen on the surface of P2 particle as indicated by arrow which possesses a central haversian canal (Hc), the canal is lined by osteoblasts (Ob), and it contain small blood vessels (Bv), (Hematoxylin—eosin stain), original magnification 400×

Control sample

Figure 14 shows a histological section of a critical size bone defect created in a rabbit femur of control group (left

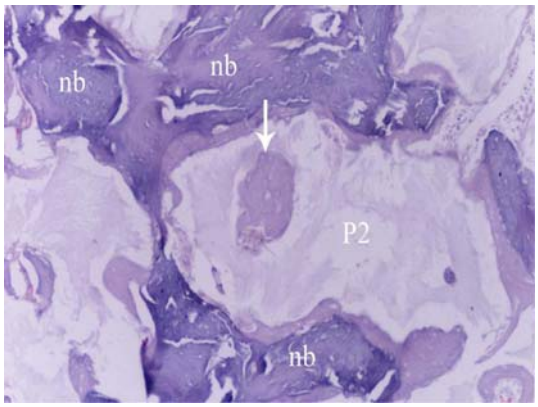

Fig. 11 A magnified image for the area inside the yellow box in Fig. 8, showing P2 particle which is surrounded completely by new bone (nb). Furthermore, bone formation is also found on the surface of P2 particle as indicated by arrow. (Hematoxylin—eosin stain), original magnification 400×

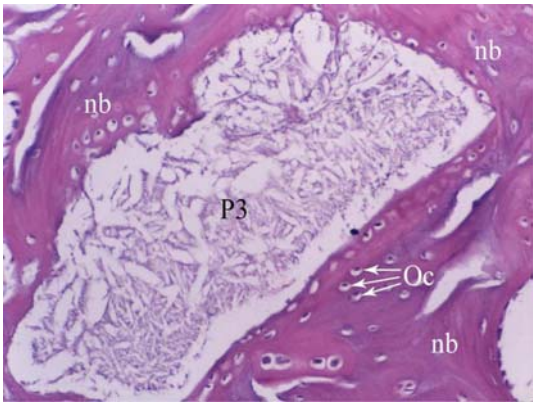

Fig. 13 A magnified image for the area inside the box in Fig. 12, showing one P3 particle which is surrounded completely by new bone (nb) with osteocyte (Oc) embeded in lacuna. (Hematoxylin—eosin stain), original magnification 200×

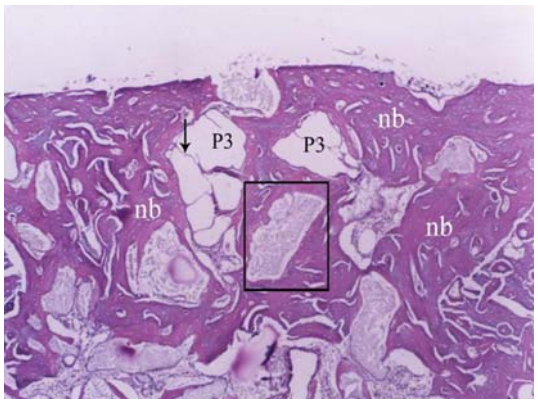

Fig. 12 Histological section of a critical size bone defect created in the rabbit femur and grafted with P3 particles 6 weeks post surgery, new bone tissue (nb) was seen filling the inter-space between the P3 particles. The in-growing bone was observed in close contact with the particles, without an intervening fibrous tissue layer. Furthermore, no sign of inflammatory cell infiltration at the implantation site were seen. Moreover, Small cracks were observed in some particles, as indicated by arrows. (Hematoxylin—eosin stain), original magnification 40×

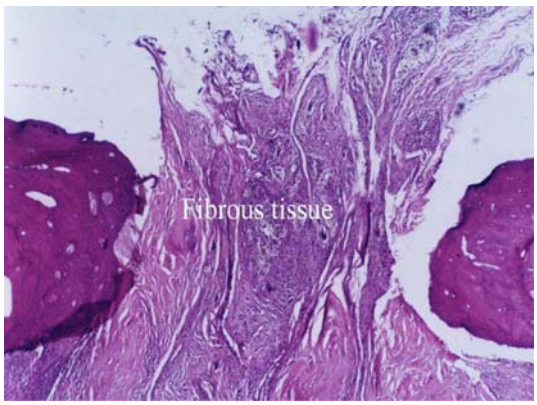

Fig. 14 Histological section of a critical size bone defect created in the rabbit femur of controlled group 6 weeks post surgery. Fibrous connective tissue was seen filling the whole area of bone defect. (Hematoxylin-eosin stain), original magnification 40×

empty with no material). Fibrous connective tissue is seen filling the whole area of bone defect. For all the grafted material used, the regeneration of bone in the defect is superior to that for the control empty defect.

Discussion

Differential thermal analysis measurements

Titanium oxide was assumed to form in phosphate glasses either TiO_5 or TiO_6 structural units [23]. The addition of TiO_2 to P_2O_5–CaO–Na_2O glass system leads to an increase in glass transition temperature (T_g), which can be interpreted by assuming that the titanate polyhedra form some new interconnections within the basic phosphate structural network. The higher bonding in the structural network results in the increase of T_g values [24]. It was assumed that, when titanium cations substitute for sodium ions, –P–$O^{\delta-}$...$Ti^{\delta+}$ bonds are formed with a strong covalent Ti–O bond than Na–O because the titanium electronegativity is larger than that of sodium [25].

From the previous considered assumptions, the increase of nucleation and crystallization temperatures with the addition of TiO_2 (as shown in Fig. 1) can be related to the higher bonding in the structural network of the glass system introduced by the incorporation of Ti–O bonds. However, the increase in nucleation and crystallization temperatures with the additions of TiO_2 is not linear as shown in Table 2. This trend indicates that the behavior of TiO_2 inside the glass network is not the same at progressive

additions. This can be related to the possible different Ti–O groups with the increase of TiO_2 content. It seems that at first titanium groups may act as former oxide (TiO_5) strengthening the network and with further addition of TiO_2, the titanium oxide enters as (TiO_6) which is probably acting as modifier oxide (TiO_6).

X-ray diffraction and scanning electron microscope measurements

The X-ray diffraction pattern of the reference sample P1 (as shown in Fig. 15) indicates that the calcium pyrophosphate (β-$Ca_2P_2O_7$) is the predominant phase in the phosphate glass-ceramics. Many authors studied the crystallization of the system P_2O_5–CaO–Na_2O. They reported that the calcium pyrophosphate phase (β-$Ca_2P_2O_7$) was formed in the glass-ceramics derived from the phosphate invert glass systems with P_2O_5 content less than 50 mol% [15, 26–29].

The glasses of the system P_2O_5–CaO–Na_2O have both Q^2 (PO_2) and Q^1 (PO_3) phosphate groups. The fraction of Q^1 groups increases proportionally to the content of the network-modifying oxides while the fraction of the Q^2 groups decreases [30]. The amount of the network-modifying oxides (Na_2O and CaO) in the present system is 55 mol%, which means that the fraction of pyrophosphate groups Q^1 is high. The crystallization of this system is expected to produce also pyrophosphate and metaphosphate crystalline phases as described in the results. Franks et al. [6] reported that the sodium metaphosphate $NaPO_3$ and sodium calcium metaphosphate $Na_4Ca(PO_3)_6$ phases were formed in the P_2O_5–CaO–Na_2O glass system with P_2O_5 content of 45 mol%. If the Na_2O content is high, sodium metaphosphate ($NaPO_3$) is the major phase and if the CaO content is high, sodium calcium metaphosphate $Na_4Ca(PO_3)_6$ is the major phase and at the intermediate compositional region the two phases are both precipitated. It seems from the results in this work that both phases are really precipitated but not as the major phases. However, the sodium metaphosphate $NaPO_3$ phase was believed to be formed with relatively high amount after the major phase of calcium pyrophosphate (β-$Ca_2P_2O_7$). The sodium calcium metaphosphate $Na_4Ca(PO_3)_6$ phase was formed with little amount. This is consistent with the author results where, in this work N_2O content is 31 mol% and CaO content is 24 mol%.

The effect of TiO_2 addition on the crystallization process (as shown in Fig. 15) was very obvious even with the addition of 0.5 mol% TiO_2. First, the peaks of the sodium calcium metaphosphate $Na_4Ca(PO_3)_6$ phase were disap-

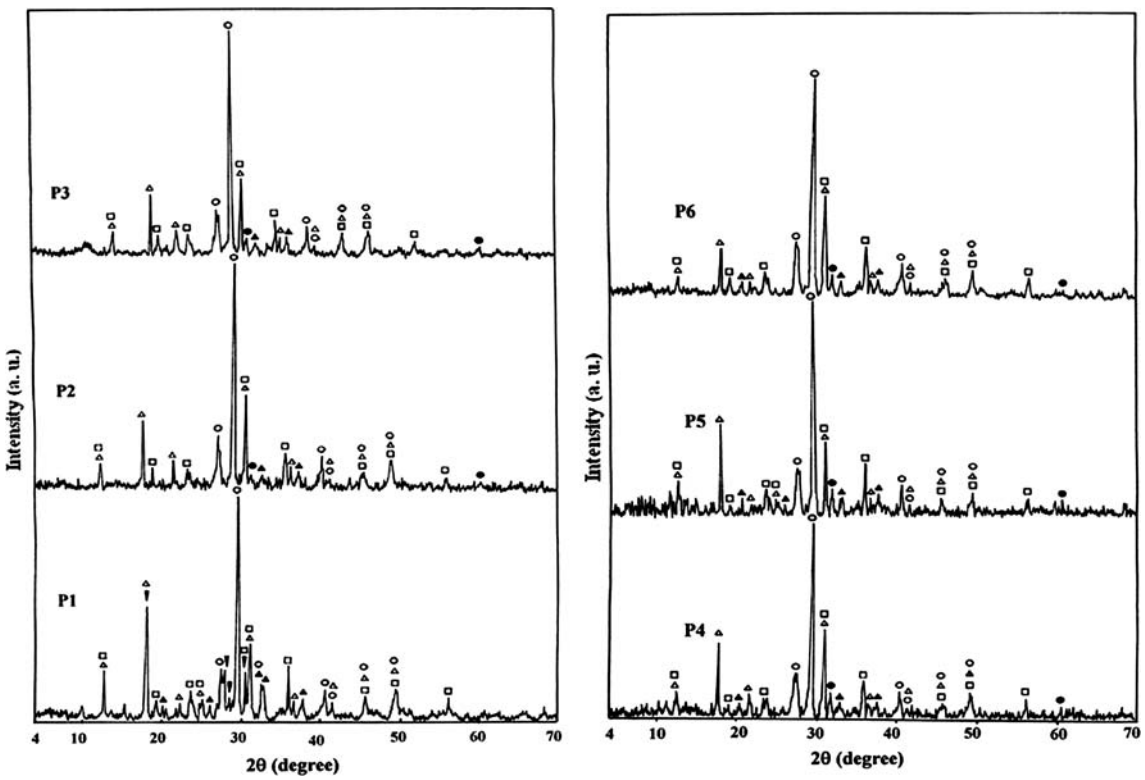

Fig. 15 X-ray diffraction patterns of the phosphate bioglass-ceramics samples [○: β-$Ca_2P_2O_7$, Δ: $NaPO_3$, □: β-$Ca(PO_3)_2$, ▲: $Na_4P_2O_7$, ▼: $Na_4Ca(PO_3)_6$, •: Na_5 Ti $(PO_4)_3$]

peared. Also, the peaks of the sodium metaphosphate $NaPO_3$ phase were lowered and new peaks of the sodium titanium phosphate $Na_5Ti(PO_4)_3$ phase were distinguished. This effect may be correlated with the depolymerization effect of TiO_2 on the metaphosphate network [24].

The depolymerization of the metaphosphate by TiO_2, is also reflected on the infrared absorption spectra of the phosphate glasses. The incorporation of titanium into a new crystalline phase does not inhibit the decrease of sodium metaphosphate $NaPO_3$ phase except in sample P5. The X-ray diffraction pattern of sample P5 reveals that the peaks of the $NaPO_3$ phase are still high. The new titanium phase in sample P5 possesses also high intensity peaks which, indicate that titanium is consumed nearly inside this phase. So, the metaphosphate phase ($NaPO_3$) is shown to increase again.

The images of the scanning electron microscope (shown in Fig. 2) show that the addition of the TiO_2 resulted in the morphological structure variations between the samples. These results indicate that TiO_2 has a pronounced effect on the crystallization process because the addition of even small quantities of TiO_2 to the base glass resulted in obvious variation of the surface texture. X-ray diffraction results indicate the effect of TiO_2 on the crystalline phases formed in the glass-ceramics which is reflected on the surface texture of the samples. By increasing the TiO_2 content, the intensity of the precipitated crystalline phases changed, where the $NaPO_3$, β-$Ca(PO_3)_2$ phases decreased while the other $Na_4P_2O_7$, $Na_4Ca(PO_3)_6$ phases nearly disappeared and a new sodium titanium phosphate $Na_5Ti(PO_4)_3$ phase was resolved.

Corrosion studies

First, it can be assumed that the dissolution of the phosphate glasses must be considered to explain the behavior of the glassy phase and the crystalline phosphate phases towards the action of aqueous solutions (i.e., SBF). Bunker et al. [31] showed that the phosphate glass dissolves congruently or uniformly which means that the dissolution products in the solution have identical composition with that of the bulk glass. The dissolution process was assumed to be divided into two kinetic periods according to the profiles of dissolved amount, q versus time, t, e.g., a decelerating dissolution period of $q \propto t^{1/2}$ and a uniform dissolution period of $q \propto t$. They showed that the hydrolysis of the linear polymeric phosphates exhibits clear pH dependence. Hydrolysis is believed to be accelerated in acids, with a fractional dependence on $[H^+]$.

Phosphate glasses dissolve in aqueous media in the following two interdependent steps [32]:

(1) Hydration reaction: the glass exchanges its sodium ions with the hydrogen ions in water to carry out Na–H ion exchange reaction, resulting in the formation of a hydrated layer on the glass surface at the glass-water interface.
(2) Network breakage: under the attack of hydrogen ions and water molecules, the P–O–P bonds in hydrated layer break up and result in the destruction of the glass network and the release of chains of phosphates with different degree of polymerization into the solution.

The glass ceramic samples consist of both crystalline phases and residual glassy phase. The corrosion of such glass-ceramic samples can be explained by considering the solubility properties of both the crystalline phases and the glassy phase. Lin et al. [33] studied the degradation of β-$Ca_2P_2O_7$ calcium pyrophosphate in distilled water and found that it is stable and inert. Antonucci et al. [34] reported that calcium metaphosphate β-$Ca(PO_3)_2$ is extremely insoluble in aqueous solutions, even in acidified aqueous media. On the other hand, sodium metaphosphate $NaPO_3$, and sodium pyrophosphate $Na_4P_2O_7$ were reported to dissolve easily in aqueous media [35]. The quite high chemical durability of calcium metaphosphate phase can be explained by considering its structure. For calcium metaphosphate β-$Ca(PO_3)_2$, the polymeric structure shows the covalently bound PO_3 units which are structurally linked through P–O–P bonds to form long metaphosphate chains. These chains are ionically bound to calcium between chains. Therefore, the divalent cations can serve as ionic cross-links between the nonbridging oxygens of two different chains. The formation of such cross-links explains the quite high chemical durability.

The X-ray diffraction data are known to provide accurate information of the crystalline phases and their evolution inside the glass-ceramic samples. Using these data and the solubility properties of the different phases, the degradation behavior of the glass-ceramic samples can thus be understood and explained. It is obvious that the effective crystalline phase in the dissolution process is sodium metaphosphate $NaPO_3$ phase because it is found in all the samples with considerable amounts (as seen from X-ray diffraction data). Also, the residual glassy phase must be taken into consideration.

For the phosphorous ions release from the phosphate bioglass-ceramic samples shown in Fig. 3, the fast release of the phosphorous ions at the early times of immersion indicates that the sodium metaphosphate crystalline phase and the residual glassy phase found on the surface dissolved rapidly into the SBF solution. Also, it is obvious that the release of phosphorous ions from the samples P1 and P5 are the highest. This can be explained by considering the crystalline phases composition of the samples which are revealed by X-ray diffraction measurements. The high

release of phosphorous ions from sample P1 is due to the absence of titanium, so the sodium metaphosphate $NaPO_3$ crystalline phase is found with high amount. Also, the X-ray diffraction results showed that the relative amount of the sodium metaphosphate $NaPO_3$ crystalline phase in sample P5 is higher than that of the rest of the samples containing titanium. Thus, the increase of the sodium metaphosphate phase obviously results in the increase of the release of the phosphorous ions from sample P5.

For the release of sodium ions from the samples shown in Fig. 4, the progressive increase of the released sodium ions indicates that the crystalline phases containing sodium ions seem to dissolve constantly. Also the data of the release of calcium ions shown in Fig. 5 indicate that the calcium ions may be released at the beginning from the residual glassy phase then reach to a maximum.

In vivo bioactivity of bioglass-ceramic samples

The bonding mechanism of calcium phosphate glass-ceramics to bone appears to be very different from the bonding of the silicate bioactive glasses. Neo et al. [21] reported that the resorbable calcium phosphate ceramics like tricalcium phosphate make direct contact with the bone, and no apatite layer was present at the interface. The surfaces of the implants become rough due to degradation, and bone grow into the finest surface irregularities. So, they suggested that the bonding strength was considered to be mainly attributable to mechanical interlocking. Kitsugi et al. [36] studied the bonding mechanism of four calcium phosphate ceramics to bone. The ceramics included calcium pyrophosphate (β-$Ca_2P_2O_7$), which is the main crystalline phase in the present work. The results of Kitsugi et al. [36] revealed that collagen fibers were not observed at the bone-ceramic interface. Neither chemical bonding nor mechanical bonding by interlocking between bone and ceramics was described by morphological observation using transmission electron microscopy.

The histological observations for the samples revealed the following features:

1) The result from sample P1 (shown in Figs. 6 and 7) which contains no titanium dioxide, shows bone growth between the particles and also on the surface of the particles. This result can be explained by referring to the presence of calcium pyrophosphate (β-$Ca_2P_2O_7$) as the main phase, which is considered as a high bioactive material [36, 37].
2) The result from sample P2 (shown in Figs. 8–11) with 0.5 mol% TiO_2 added to its parent glass shows bone growth between the particles and on the surface of the particles like sample P1 but with advanced stages of bone growth which means that the sample P2 is relatively more bioactive than sample P1. The effect of the addition of 0.5 mol% TiO_2 on the crystallization process may be the reason. The $NaPO_3$, β-$Ca(PO_3)_2$ phases decreased and the other phases $Na_4P_2O_7$, $Na_4Ca(PO_3)_6$ nearly disappeared and a new phase $Na_5Ti(PO_4)_3$ appeared with very small amount. The relative decrease of the other phases which was found in the sample P1 may be the reason for the improvement the bioactivity of the sample P2.
3) By increasing the percentage of TiO_2 in the other samples P3–P6, the results (shown in Figs. 12 and 13) showed bone growth between the particles only. This means that the addition of 1 mol% TiO_2 or more to the parent phosphate glass P1 will be expected to decrease the bioactivity. This observation can be explained by the observed increase of the chemical durability of the samples caused by the introduction of TiO_2. However the sample P5 with 2 mol% TiO_2 showed high release of phosphorous ions like the sample P1 and the amount of crystalline $NaPO_3$ phase in the sample is considered high. The histological results for this sample P5 show that the bone growth was better than that of the samples P3, P4, and P6. However, there is no bone growth on the surface of the particles of the sample P5 like the sample P1 and P2. It can thus be concluded from these results that the degradation of the samples is not only the important factor for the bioactivity but the composition of the phosphate glass-ceramics also plays an important role for the bone growth on the material. The low content of TiO_2 in the sample P2 has no negative effect on its bioactivity as indicated from the in vivo results. At the same time, the action of TiO_2 in sample P2 on the crystallization process seems to improve the bioactivity of the sample.

Conclusion

The bioactivity of the glass-ceramic samples differs by the amount of TiO_2 added to the parent glass. The addition of 0.5 mol% TiO_2 gave an increased bioactivity due to the action of TiO_2 on the crystallization process, where the other crystalline phases than the calcium pyrophosphate crystalline phase are decreased. By the addition of 1, 1.5, 2.5 mol% TiO_2, the bioactivity decreased due to the increase of the chemical durability. By the addition of 2 mol% TiO_2, the degradation increased due to the increase of the sodium metaphosphate phase ($NaPO_3$). However, the bioactivity of the sample was still low in relative to the base sample (without addition of TiO_2). This means that the degradation is not the only important factor for the bioactivity but the presence of other crystalline phases than

bioactive calcium pyrophosphate crystalline phase can affect the bioactivity. A main conclusion is that the calcium pyrophosphate crystalline phase induces the bone growth without need for chemical bonding.

Acknowledgement We would like to express our gratitude to Dr. A. Elkady for her generous help.

References

1. L. L. HENCH, *J. Am. Ceram. Soc.* **81** (1998) 1705
2. J. C. KNOWLES and G. W. HASTINGS, *J. Mater. Sci. Mater. Med.* **4** (1993) 102
3. P. Y. SHIH, S. W. YUNG and T. S. CHIN, *J. Non-Cryst. Solids* **224** (1998) 143
4. X. J. XU, D. E. DAY, R. K. BROW and P. M. CALLAHAN, *Phys. Chem. Glasses* **36** (1995) 264
5. B. C. SALES, R. S. RAMSEY, J. B. BATES and L. A. BOATNER, *J. Non-Cryst. Solids* **87** (1986) 137
6. K. FRANKS, I. ABRAHAMS, G. GEORGIOU and J. C. KNOWLES, *Biomaterials* **22** (2001) 497
7. V. SALIH, K. FRANKS, M. JAMES, J. M. HASTINGS, J. C. KNOWLES and J. OLSEN, *J. Mater. Sci. Mater. Med.* **11** (2000) 615
8. P. W. MCMILLAN, Glass-ceramics, 2nd edn (Academic Press: London, 1979)
9. W. VOGEL, Glass chemistry (Springer: Berlin, 1994)
10. Y. NAN, W. E. LEE and P. F. JAMES, *J. Am. Ceram. Soc.* **75** (1992) 1641
11. P. F. JAMES, *J. Non-Cryst. Solids* **181** (1995) 1
12. H. HOSONO, Z. ZHANG and Y. ABE, *J. Am. Ceram. Soc.* **72** (1989) 1587
13. H. HOSONO and Y. ABE, *J. Non-Cryst. Solids* **190** (1995) 185
14. S. R. LACERDA, J. M. OLIVEIRA, R. N. CORREIA and M. H. V. FERNANDES, *J. Non-Cryst. Solids* **221** (1997) 255
15. T. KASUGA, M. SAWADA, M. NOGAMI and Y. ABE, *Biomaterials* **20** (1999) 1415
16. T. KASUGA, Y. HOSOI, M. NOGAMI and M. NIINOMI, *J. Am. Ceram. Soc.* **84** (2001) 450
17. H. GRUSSAUTE, L. MONTAGNE, G. PALAVIT and J. L. BERNARD, *J. Non-Cryst. Solids* **263&264** (2000) 312
18. M. NAVARRO, M.-P. GINEBRA, J. CLEMENT, M. SALVADOR, A. GLORIA and J. A. PLANELL, *J. Am. Ceram. Soc.* **86** (2003) 1345
19. S. LANGSTAFF, M. SAYER, T. J. N. SMITH, S. M. PUGH, S. A. M. HESP and W. T. THOMPSON, *Biomaterials* **20** (1999) 1727
20. S. KOTANI, Y. FUJITA, T. KITSUGI, T. NAKAMURA, T. YAMAMURO, C. OHTSUKI and T. KOKUBO, *J. Biomed. Mater. Res.* **25** (1991) 1303
21. M. NEO, S. KOTANI, Y. FUJITA, T. NAKAMURA, T. YAMAMURO, Y. BANDO, C. OHTSUKI and T. KOKUBO, *J. Biomed. Mater. Res.* **26** (1992) 255
22. T. KOKUBO, H. KUSHITANI, S. SAKKA, T. KITSUGI and T. YAMAMURO, *J. Biomed. Mater. Res.* **24** (1990) 721
23. R. K. BROW, D. R. TALLANT, W. L. WARREN, A. MCINTYRE and D. E. DAY, *Phys. Chem. Glasses* **38** (1997) 300
24. L. KOUDELKA, P. MOSNER, M. ZEYER and C. JAGER, *J. Non-Cryst. Solids* **326&327** (2003) 72
25. A. SHAIM, M. ET-TABIROU, L. MONTAGNE and G. PALAVIT, *Mater. Res. Bull.* **37** (2002) 2459
26. W. VOGEL and W. HOLAND, *Angew. Chem. Int. Ed. Engl.* **26** (1987) 527
27. J. ALKEMPER and H. FUESS, *J. Non-Cryst. Solids* **210** (1997) 32
28. I. ABRAHAMS, G. E. HAWKES and J. C. KNOWLES, J. Chem. Soc. Dalton Trans. (1997) 1483
29. Y. ZHANG and J. D. SANTOS, *J. Non-Cryst. Solids* **272** (2000) 14
30. P. HARTMANN, J. VOGEL and B. SCHNABEL, *J. Non-Cryst. Solids* **176** (1994) 157
31. B. C. BUNKER, G. W. ARNOLD and J. A. WILDER, *J. Non-Cryst. Solids* **64** (1984) 291
32. H. GAO, T. TAN and D. WANG, *J. Control. Release* **96** (2004) 29
33. F.-H. LIN, C.-J. LIAO, K. S. CHEN, J.-S. SUN and H.-C. LIU, *Biomaterials* **18** (1997) 915
34. J. M. ANTONUCCI, B. O. FOWLER and S. VENZ, *Dent. Mater.* **7** (1991) 124
35. D. R. LIDE, CRC handbook of physics and chemistry (CRC Press: Boca Raton, 2004)
36. T. KITSUGI, T. YAMAMURO, T. NAKAMURA and M. OKA, *Biomaterials* **16** (1995) 1101
37. T. KITSUGI, T. YAMAMURO, T. NAKAMURA, S. KOTANI, T. KOKUBO and H. TAKEUCHI, *Biomaterials* **14** (1993) 216